IOP Publishing Journal Title
Journal **XX** (XXXX) XXXXXX https://doi.org/XXXX/XXXX

Photoresponse of wafer-scale palladium diselenide films prepared by selenization method

Chun Hin Mak, Shenghuang Lin, Lukas Rogée and Shu Ping Lau

Department of Applied Physics, The Hong Kong Polytechnic University, Hung Hom, Kowloon, Hong Kong SAR

E-mail: apsplau@polyu.edu.hk

Received xxxxxx
Accepted for publication xxxxxx
Published xxxxxx

Abstract

Palladium diselenide ($PdSe_2$) films exhibit a high charge carrier mobility and sensitivity in photodetection. In this work, wafer-scale $PdSe_2$ thin films with controllable thickness have been synthesized by the selenization of Pd films. A $PdSe_2$-based photodetector can detect a broad wavelength ranging from 420 nm to 1200 nm. The responsivity and detectivity can reach 1.96×10^3 A W^{-1} and 1.72×10^{10} W / $Hz^{1/2}$ at $V_{SD} = 3$ V, respectively. The figure of merit of the photodetection are comparable to the mechanically exfoliated $PdSe_2$ based photodetector. This work demonstrated that selenization is a facile method to synthesize $PdSe_2$ films in large scale and the films are promising for broadband photodetection.

Keywords: palladium diselenide, two-dimensional layered material, photodetection, field effect transistors

Introduction

After graphene was discovered in 2004,[1] the research of two-dimensional layered materials (2DLMs) have been raised. Some 2DLMs exhibit layer-dependent bandgap[2] and hence their spectral absorption can be tuned by controlling their thickness. For instance, MoS_2 has a band gap transition from indirect band gap value of about 1.2 eV to direct band gap of 1.8 eV by reducing the thickness from bulk to monolayer,[3–8] while black phosphorus (BP) has a band gap transition from 0.3 eV to 2 eV.[9] Also, under the field effect transistors architecture, the MoS_2 and BP flakes showed layer-dependent charge carrier mobility and photoresponse under light illumination.[10] Similar layer-dependent properties are also found in other 2D semiconductors and semimetals such as WS_2, $MoSe_2$ and $PtSe_2$.[11–13] Combining the high electrical performance and the vast choices of materials for optical absorption, which make 2DLM family suitable for photodetector applications.[2,14,15]

The application of the 2DLM-based field effect transistors (FETs) is suffering from non-scalable production. Until now, most of the FETs were based on the exfoliation of bulk crystals. In most of these works, the dimensions of the flakes are usually within the range of several hundred microns.[16–22] For the next generation photodetectors, a better controllability on thickness, area and shape are required.[14] In this aspect, sulfurization and selenization of metal precursor films show a trade-off between material quality and large-area with controllable thickness. This fabrication method has already showed its advantages in noble metal based 2DLMs such as $PtSe_2$ and $PdSe_2$.[12,23–25]

Among the transition metal dichalcogenide family, $PdSe_2$ has a unique in-plane pentagonal crystal structure.[30] As a high mobility semiconductor/semimetal, the $PdSe_2$-based photodiode demonstrated excellent performance.[24,28] The research on large-area $PdSe_2$ films is still scarce. In this work, the $PdSe_2$ films were fabricated by selenization of Pd films. The films exhibited homogeneous semi-transparency across a 2" sapphire substrate. A broad photodetection ranging from 420 nm to 1200 nm was demonstrated. A high responsivity of 1.96×10^3 AW^{-1} for 980 nm was also achieved.

Experimental Section

Chemicals and substrates:

Selenium powder (99.99%) was purchased from Sigma Aldrich. Polished 2'' in diameter c-plane (0001) sapphire wafer and polished 4'' SiO_2/Si (500 nm thick) were purchased from Silicon Valley Microelectronics, Inc.

$PdSe_2$ film fabrication method:

Palladium (Pd) films on sapphire substrates were prepared by a DC magnetron sputtering system. The 99.95 % purity Pd target was used. After the pressure of the chamber reached 1×10^{-6} Torr, argon gas was introduced, and the pressure was kept at 5×10^{-3} Torr. The deposition power was 10 W during the Pd deposition. The deposition time was adjusted to control the Pd thickness and hence the thickness of the $PdSe_2$ samples.

During the selenization process, the substrates were placed inside the heat zone of a tube furnace and the selenium powders were placed upstream and 15 cm apart from the substrates. The argon gas flow rate was 90 sccm and the pressure was kept at 5 Torr. The temperature of the substrates and Se powder were kept at 350 ºC and 300 ºC, respectively.

Fabrication of $PdSe_2$ transistor:

A thin layer of polystyrene (PS) was deposited on the $PdSe_2$ by spin-coating. To ensure the cleanliness and the intrinsic performance of the $PdSe_2$, the PS/$PdSe_2$ composite was peeled off by allowing deionized water to penetrate into the interface between $PdSe_2$ and sapphire slowly. The as-synthesized $PdSe_2$ thin films were then wet-transferred on a SiO_2/Si with pre-defined Cr/Au electrode. The film was further annealed at 120 ºC for 30 minutes for better contact. Finally, toluene was used to remove the PS under ambient conditions and the $PdSe_2$ transistors were ready to use.

Electrical measurement of $PdSe_2$ transistor:

All the electrical measurements were carried out with a Keithley 4200-SCS at room temperature in a nitrogen filled glove box with O_2 and H_2O < 10 ppm. For photodetection, the light emitting diodes with emission wavelengths of 420 nm, 530 nm, 895 nm, 980 nm and 1200 nm were used to illuminate the transistor channel.

Materials characterization:

High resolution transmission electron microscopy (HRTEM), selected area electron diffraction (SAED) and energy-dispersive X-ray spectroscopy (EDX) measurements were performed by JEOL JEM-2100F Field Emission Electron Microscope. Carbon coated copper grids were used as sample holders. X-ray diffraction (XRD) measurement was conducted by the Rigaku SmartLab X-ray Diffractometer. Raman spectroscopy of $PdSe_2$ was measured by LabRAM HR 800 Raman Spectrometer. Thickness measurements were determined by atomic force microscope (AFM, Asylum MFP-3D Infinity). The UV-vis-NIR absorption spectroscopy was obtained by Perkin Elmer LAMBDA 1050 UV/Vis Spectrophotometer.

Results and discussion

Figure 1a shows the photograph of a sapphire substrate, sputtered Pd film and the selenized $PdSe_2$ film. The Pd and $PdSe_2$ films are semi-transparent and PdSe is darker. The temperature profile of selenization in tube furnace and the calibration curve of the $PdSe_2$ thickness against the sputtering time are shown in **Figure S1a** and **S1b** (Supporting Information), respectively. **Figure S2** provides the AFM images of the film thickness. The thicknesses are about 1.7 nm, 4.9 nm, 9.2 nm, 10.4 nm with the Pd deposition time of 15 s, 30 s, 60 s, 75 s, respectively. **Figure 1b** shows the Raman scattering spectra under the 433 nm laser excitation. The Raman modes of A_g^1 (≈ 143 cm^{-1}), A_g^2 (≈ 206 cm^{-1}), B_{1g} (≈ 222 cm^{-1}) and A_g^3 (≈ 256 cm^{-1}) are well consistent with the literature.[26,29] The peak intensity was also varied with the thickness of the $PdSe_2$. **Figure 1c** shows the intensity ratio of A_g^1/A_g^3, it decreases as the thickness increases.

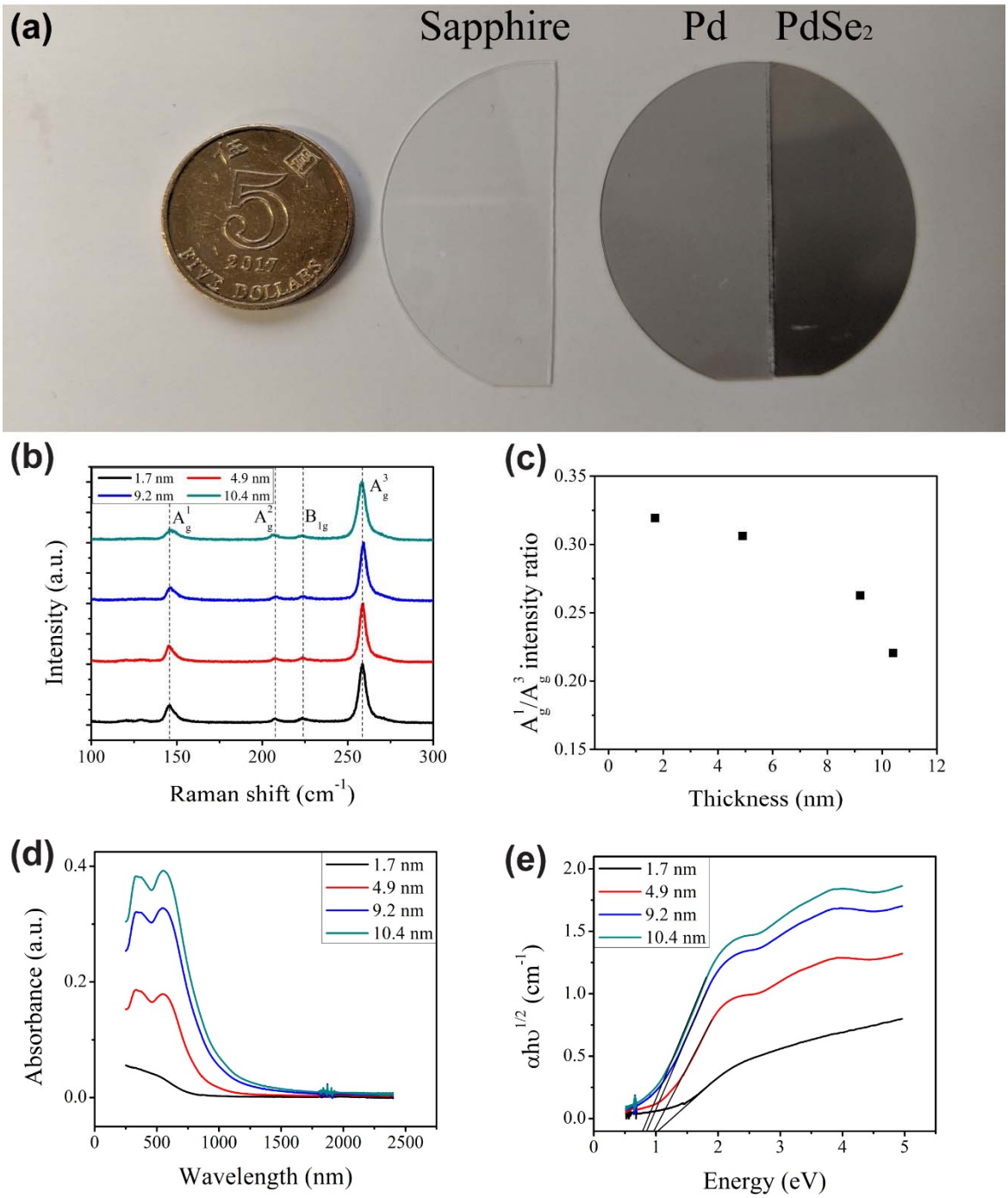

Figure 1(a) The photographs of sapphire substrate, Pd and $PdSe_2$ on sapphire. (b) The Raman scattering of the films with various thickness. (c) the ratio of A_g^1/A_g^3 with various thickness. (d) The UV – vis – NIR absorption spectra and (e) the tauc plot of the $PdSe_2$ films.

The ratio could serve as an indicator of $PtSe_2$ film thickness. Similar result was also found in the literature.[23] The UV – vis – NIR absorption spectra of the $PdSe_2$ films on sapphire are shown in **Figure 1d**. The absorbance and absorption range can be enhanced by increasing the thickness. Besides, there exists two obvious absorption peaks at 330 nm and 558 nm in the films which thickness reaches 4.9 nm or above. **Figure 1e** shows the Tauc plot of the samples. The optical band gap of the films decreases as the film thickness increases. The bandgap of the $PdSe_2$ films is thickness dependent.

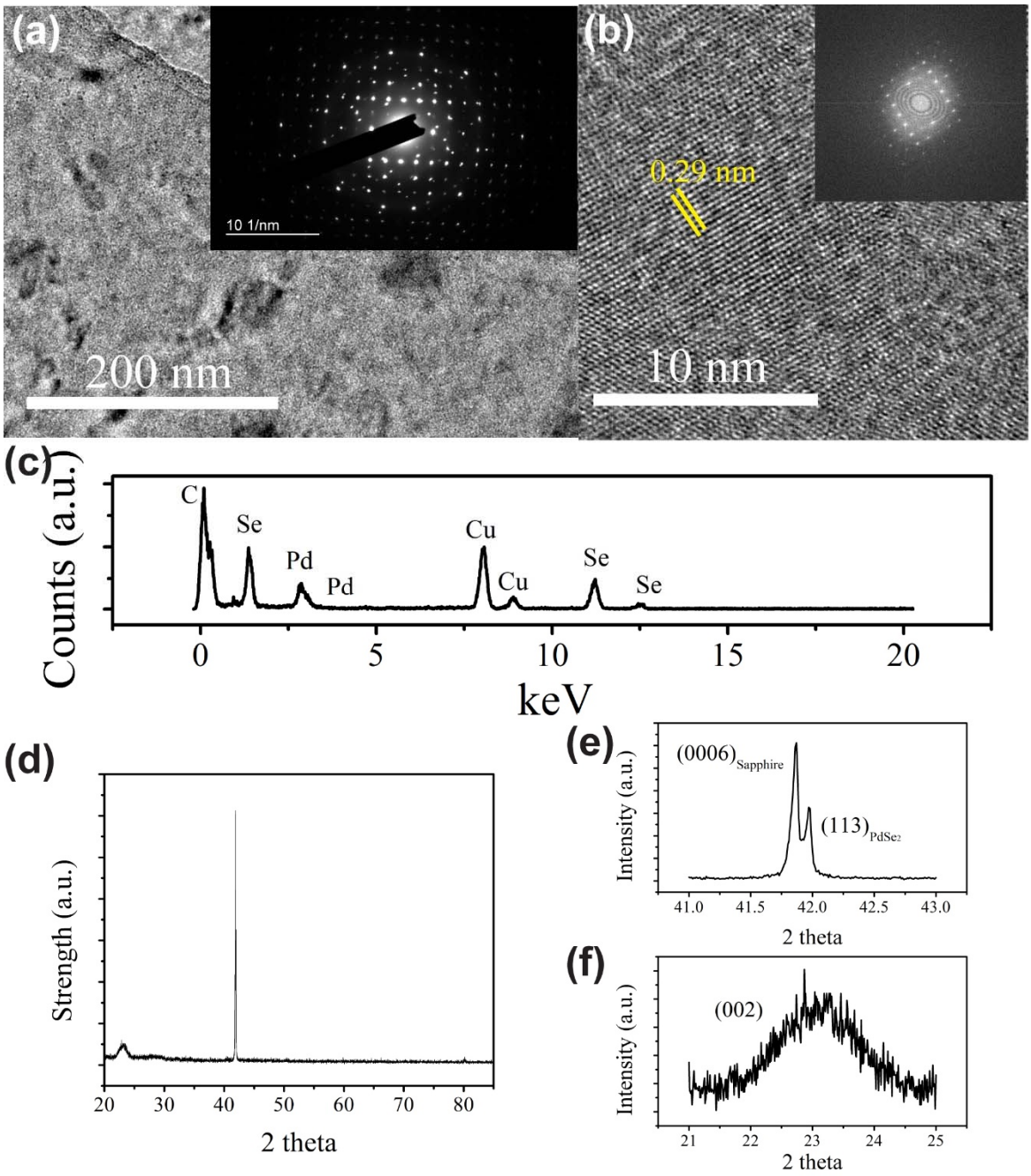

Figure 2 Material characterization of the 9.2 nm-thick $PdSe_2$ film. (a) The TEM image and SAED pattern (inset) of the film. (b) The HRTEM image and FFT (inset) of the film. (c) EDX spectrum of the film measured on the carbon coated copper grid. (d) XRD of the films. Enlarged XRD spectrum of (e) 41° to 43° and (f) 21° to 25°.

The 9.2-nm-thick $PdSe_2$ film was selected to conduct TEM and XRD measurements. **Figure 2a** shows the TEM image of the film with the SAED pattern is shown in the inset. SAED patterns were randomly selected on the copper grid to investigate the crystallinity of the films in a microscopic view. The regular spot sequences with superimposition of the rings patterns are shown. The superimposition implies the film is polycrystalline. The crystal quality is comparable to the previous sulfurization/selenization works.[25,30] The HRTEM image of the film is shown in **Figure 2b.** The lattice constant of 0.29 nm is consistent with the (200) planes of the previous reported $PdSe_2$ film.[31] Moreover, the EDX spectrum of the film was acquired during the TEM measurement. It shows the signals of carbon, copper,

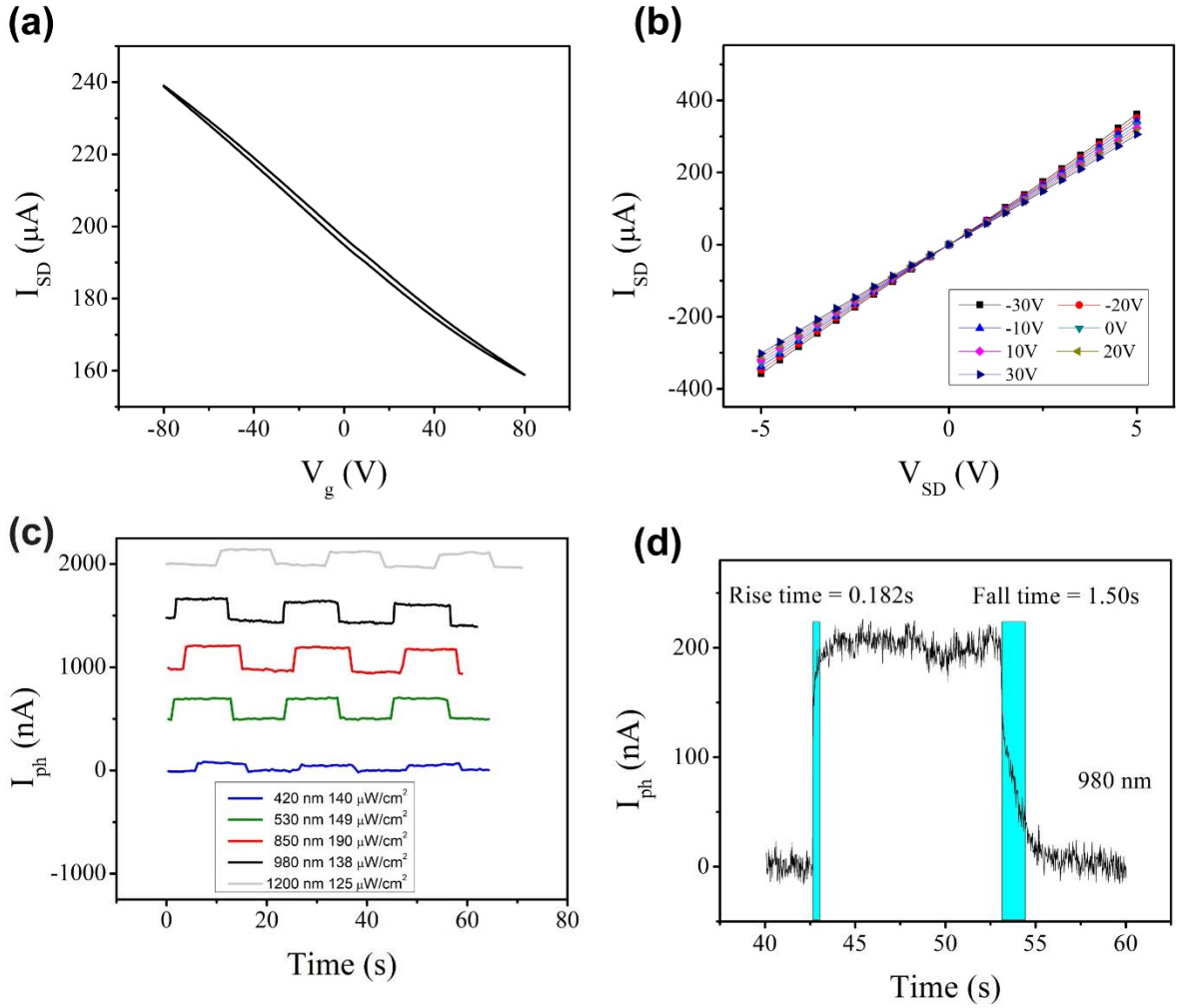

Figure 3 The electrical and light detection performance of the 9.2 nm – thick $PdSe_2$ transistors. (a) Dual sweep transfer characteristics curve and (b) output characteristics curve, (c) the photocurrent of the transistor under different light wavelength. The offsets of 500 nA, 1000 nA, 1500 nA and 2000 nA are added to separate the data of photoresponses. (d) the response time of device under 980 nm (Intensity : 138 μW / cm^2).

The stoichiometric ratio of the film was investigated by filtering the signals of carbon and copper. The remaining atomic ratio of Pd:Se is close to 1:2. No other elements can be found in the spectrum. Furthermore, the film on sapphire was measured by XRD. **Figure 2d-2f** show the broad range and magnified XRD spectrum. The (002) (≈ 22°) and (113) (≈ 41.9°) peaks matches the XRD peaks of single crystal $PdSe_2$. The average crystal domain size of the (113) plane is about 148 nm according to the Scherrer formula D = (0.94 λ) / (β cosθ), where D = average crystallite size, β = FWHM in radians, θ = Bragg angle, λ = 0.154 nm.

Meanwhile, bottom gate FET configuration was further employed to investigate the transport properties of the 9.2 nm – thick $PdSe_2$ film. **Figure 3a** and **3b** shows the dual sweep transfer and output characteristics curves of the $PdSe_2$ FET. The transfer characteristic curve shows the p-type characteristic with an on/off ratio of 1.50 under the sweep of gate voltage. Since the measurements were conducted in a nitrogen filled glove box with O_2 and H_2O concentration < 0.1 ppm, trappings from surface adsorbate were eliminated. The small hysteresis of the transistor indicates that the intrinsic traps of the polycrystalline $PdSe_2$ do not hinder the movement of the charge carriers effectively. The output characteristic curves show a typical resistance change of semiconductor channel in FET structure under different gate voltages. The field effect mobility μ =1.20 cm^2 V^{-1} s^{-1} was calculated according to the equation:[32,33]

$$\mu = \frac{L}{WC_{OX}V_{ds}} \times \frac{dI_{DS}}{dV_g} \quad (1)$$

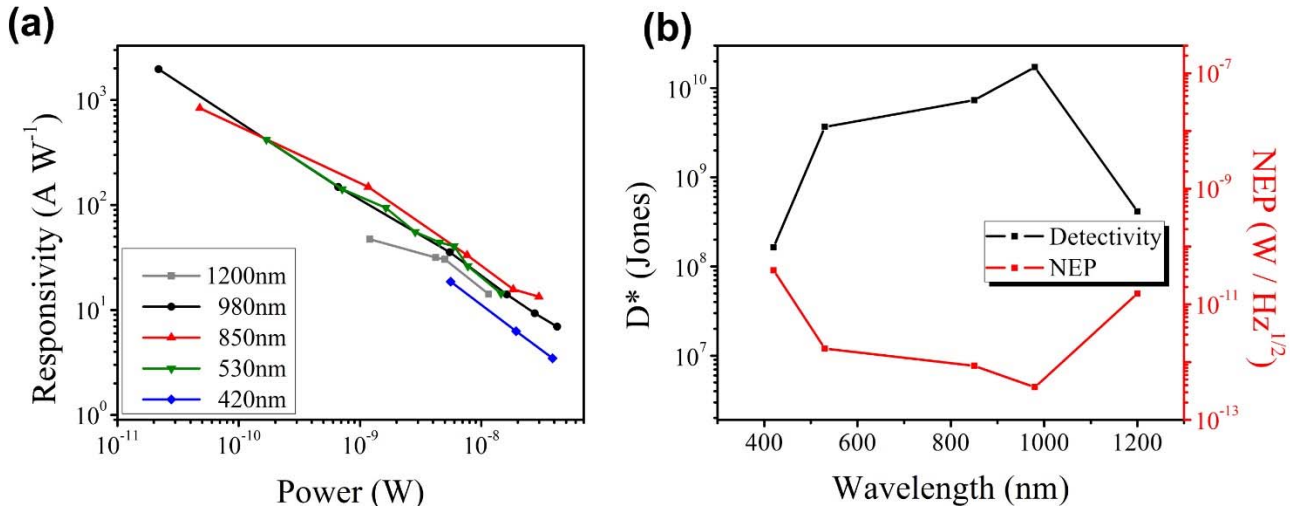

Figure 4 (a) The responsivity of the 9.2 nm – thick $PdSe_2$ transistors. (b) The specific detectivities (D*) and noise equivalent powers (NEP) of the 9.2 nm – thick transistors.

where channel length L and width W is 5 μm and 800 μm respectively, the capacitance C_{ox} ($C_{ox} = \varepsilon_0\varepsilon_r/d$, $\varepsilon_0 = 8.854 \times 10^{-12}$ F m^{-1}, ε_r for SiO_2 is 3.9, and SiO_2 thickness d = 300 nm) and V_{SD} = 3V.[2]

The FET was then tested for photodetection under V_{SD} = 3V and V_g = 0V. The light emitting diodes (LEDs) with wavelengths of 420 nm, 530 nm, 850 nm, 980 nm and 1200 nm were served as the light sources. During light illumination, the $PdSe_2$ channel absorbs photon energy and generates electron-hole-pairs (EHPs). The voltage bias V_{SD} will separate the electron and holes to different electrodes and the photocurrent will be detected. The device shows a broadband photoresponse from 420 nm to 1200 nm. The photocurrents (the difference of the currents with and without light illumination) are shown in **Figure 3c.** They show the stable photocurrent change under the same light intensity illumination. A rise time of 182 ms and decay time of 1.50 s was recorded (**Figure 3d)**. The log-log plots of the photocurrent and power are shown in the **Figure S4**. Under different sensing wavelengths, the log-log plots show the linear relationship between I_{ph} and P. Hence the typical $I_{ph} \propto P^{\beta}$ relationship can be experimentally established. The β values in the plots are ranging from 0.13 to 0.49 and less than the ideal value 1. The results indicate that there are loss of photocurrent in the transistor.[34] However, it is reasonable that the polycrystalline $PdSe_2$ has material defects, the defect sites would act as the recombination location of photogenerated carrier.[35–37]

As the figure of merit in photodetection, responsivity R, and specific detectivity D* were calculated. The responsivity R of the FET under the illumination of the aforementioned lights was then calculated by:

$$R = \frac{I_{ph}}{P} = P^{\beta-1} \quad (2)$$

where P is the illuminated power and I_{ph} is the photocurrent. I_{ph} is deduced by the subtraction of the currents with and without light illumination. Among all the testing conditions, the highest responsivity is found to be 1.96×10^3 A W^{-1} when 980 nm light with a power of 22 pW is used. The lowest responsivity is recorded (3.47 A W^{-1}) when 420 nm light is used. **Figure 4a** shows the photoresponsibility of the device at various wavelengths. The responsivities show the linear relationship in the log-log plot of responsivity and power, which are also in agreement with Equation (2). The gain of the transistor is about 2.48×10^3,which is estimated by the equation:[38]

$$G = \frac{I_{ph}}{P} \times \frac{E}{q\eta} \quad (3)$$

where E is the photon energy of the incident light, η is the external quantum efficiency (assuming 100%) and q is the elementary charge.

The specific detectivity D* is another figure of merit of the photodetectors. To evaluate the D* values of the FET under different light intensities and wavelengths, the following equations for D* and noise equivalent power NEP are employed:[39]

$$NEP = \frac{i_{n,rms}}{R} \quad (4)$$

and $$D^* = \frac{\sqrt{AB}}{NEP} = \frac{R\sqrt{AB}}{i_{n,rms}} \quad (5)$$

where A is the effective illuminated area of the channel = 4 × 10^{-7} cm^{-2}, B is the bandwidth, $i_{n,rms}$ is the root mean square value of the noise current and R is the responsivity of the device. Since 1/f noise was shown to be the most dominant noise source in 2DLM transistors,[14,40] the noise level $i_{n,rms}$ of the $PdSe_2$ FET was found by the Fourier transform (FFT) of the measured dark current (**Figure S5**) and was about ≈ 722 $pAHz^{-1/2}$ per unit bandwidth (B = 1 Hz). The maximum D* and their corresponding NEP values of different wavelengths are plotted in **Figure 4b**. The FET shows the highest specific detectivity in the sensing range 420 nm to 1200 nm within the values of 1.63 × 10^8 to 1.72 × 10^{10} Jones. The D* values are similar to other reported 2DLM transistors.[41]

According to the $PdSe_2$ transistors fabricated by mechanical exfoliation, they exhibited better photoresponse and responsivity in NIR region than the visible light spectrum.[28,42] Although the polycrystalline structure of our $PdSe_2$ inevitably increases the free charge carriers from the defects and hence the conductivity, which result in a relatively low on/off ratio. However, the transistor also shows a improved photoresponse in NIR region than the visible light region. Moreover, our $PdSe_2$ transistor shows similar responsivity and detectivity values to them. The reported responsivity and detectivity of $PdSe_2$ transistor were about 708 A W^{-1} and 8.2×10^9 Jones at the wavelength of 1064 nm,[42] while our responsivity and detectivity of $PdSe_2$ transistor is 1960 A W^{-1} and 1.72 × 10^{10} Jones at the wavelength of 980 nm. It has been reported that some of the 2DLM photodetectors could achieve high responsivity which is attributed to long life time of the photocarriers, but not high mobility. Thus it will lead to a long response time in photodetection.[14] However, as indicated by the aforementioned β values which are smaller than 1, the material defects in polycrystalline materials will act as the recombination center of the photocarriers and reduce the average life time. Regarding to this issue, although the thickness and synthesis are different, T**able 1** shows our results with other large area $MoSe_2$, WSe_2, MoS_2, $SnSe_2$ and ReS_2 phototransistors with similar device architecture.[43–48] Our device exhibits a good balance between high responsivity and fast response time with the broadest detection range.

Table 1 Typical performance of the photodetectors with large area 2DLMs. (1L: 1 layer, FL: few layers, CVD: chemical vapor deposition)

Channel	Fabrication method	Response Time (ms)	R (AW^{-1})	Detection range (nm)	Reference
9.2 nm $PdSe_2$	Selenization	182 (rise), 1500 (fall)	1960	420 – 1200	This work
FL $MoSe_2$	CVD	400	93.7	638	43
1L WSe_2	CVD	1000	1.1	532	44
1L MoS_2	CVD	1000	0.0011	488, 514.5	45
1L MoS_2	CVD	220000	2200	532	46
FL $SnSe_2$	CVD	100000	1.9	800	47
1L ReS_2	CVD	100000	16.14	633	48

Conclusion

We successfully synthesized large area polycrystalline $PdSe_2$ by selenization of Pd films. The crystallinity, electrical and optoelectronic properties of $PdSe_2$ were shown to be suitable for photodetection. The responsivity of the $PdSe_2$ phototransistors can reach 1960 AW^{-1} under the 980 nm illumination with relatively fast response time. Our work suggests that $PdSe_2$ is a promising material for broadband photodetection.

Acknowledgements

CHM acknowledges the support of the Hong Kong PhD Fellowships scheme. This work was financially supported by a PolyU grant (1-ZVGH). The authors acknowledge Prof. Feng Yan for device characterization.

Competing financial interests

The authors declare no competing financial interests.

ORCID iDs

References

1. Novoselov, K.S., Geim, A.K., Morozov, S.V., Jiang, D., Zhang, Y., Dubonos, S.V., Grigorieva, I.V. and Firsov, A.A., 2004. Electric field effect in atomically thin carbon films. science, 306(5696), pp.666-669.

2. Xie, C., Mak, C., Tao, X. and Yan, F., 2017. Photodetectors based on two-dimensional layered materials beyond graphene. Advanced Functional Materials, 27(19), p.1603886.

3. Han, S.W., Kwon, H., Kim, S.K., Ryu, S., Yun, W.S., Kim, D.H., Hwang, J.H., Kang, J.S., Baik, J., Shin, H.J. and Hong, S.C., 2011. Band-gap transition induced by interlayer van der Waals interaction in MoS 2. Physical Review B, 84(4), p.045409.

4. Mak, K.F., Lee, C., Hone, J., Shan, J. and Heinz, T.F., 2010. Atomically thin MoS 2: a new direct-gap semiconductor. Physical review letters, 105(13), p.136805.

5. Splendiani, A., Sun, L., Zhang, Y., Li, T., Kim, J., Chim, C.Y., Galli, G. and Wang, F., 2010. Emerging photoluminescence in monolayer MoS2. Nano letters, 10(4), pp.1271-1275.

6. Eda, G., Yamaguchi, H., Voiry, D., Fujita, T., Chen, M. and Chhowalla, M., 2011. Photoluminescence from chemically exfoliated MoS2. Nano letters, 11(12), pp.5111-5116.

7. Radisavljevic, B., Radenovic, A., Brivio, J., Giacometti, V. and Kis, A., 2011. Single-layer MoS2 transistors. Nature nanotechnology, 6(3), p.147.

8. Lee, H.S., Min, S.W., Chang, Y.G., Park, M.K., Nam, T., Kim, H., Kim, J.H., Ryu, S. and Im, S., 2012. MoS2 nanosheet phototransistors with thickness-modulated optical energy gap. Nano letters, 12(7), pp.3695-3700.

9. Wang, X., Jones, A.M., Seyler, K.L., Tran, V., Jia, Y., Zhao, H., Wang, H., Yang, L., Xu, X. and Xia, F., 2015. Highly anisotropic and robust excitons in monolayer black phosphorus. Nature nanotechnology, 10(6), p.517.

10. Li, L., Yu, Y., Ye, G.J., Ge, Q., Ou, X., Wu, H., Feng, D., Chen, X.H. and Zhang, Y., 2014. Black phosphorus field-effect transistors. Nature nanotechnology, 9(5), p.372.

11. Zhang, Y., Zhang, Y., Ji, Q., Ju, J., Yuan, H., Shi, J., Gao, T., Ma, D., Liu, M., Chen, Y. and Song, X., 2013. Controlled growth of high-quality monolayer WS2 layers on sapphire and imaging its grain boundary. ACS nano, 7(10), pp.8963-8971.

12. Wang, Y., Li, L., Yao, W., Song, S., Sun, J.T., Pan, J., Ren, X., Li, C., Okunishi, E., Wang, Y.Q. and Wang, E., 2015. Monolayer PtSe2, a new semiconducting transition-metal-dichalcogenide, epitaxially grown by direct selenization of Pt. Nano letters, 15(6), pp.4013-4018.

13. Yu, X., Yu, P., Wu, D., Singh, B., Zeng, Q., Lin, H., Zhou, W., Lin, J., Suenaga, K., Liu, Z. and Wang, Q.J., 2018. Atomically thin noble metal dichalcogenide: a broadband mid-infrared semiconductor. Nature communications, 9(1), p.1545.

14. Konstantatos, G., 2018. Current status and technological prospect of photodetectors based on two-dimensional materials. Nature communications, 9(1), p.5266.

15. Bhimanapati, G.R., Lin, Z., Meunier, V., Jung, Y., Cha, J., Das, S., Xiao, D., Son, Y., Strano, M.S., Cooper, V.R. and Liang, L., 2015. Recent advances in two-dimensional materials beyond graphene. ACS nano, 9(12), pp.11509-11539.

16. Konstantatos, G., Badioli, M., Gaudreau, L., Osmond, J., Bernechea, M., De Arquer, F.P.G., Gatti, F. and Koppens, F.H., 2012. Hybrid graphene–quantum dot phototransistors with ultrahigh gain. Nature nanotechnology, 7(6), p.363.

17. Kufer, D., Nikitskiy, I., Lasanta, T., Navickaite, G., Koppens, F.H. and Konstantatos, G., 2015. Hybrid 2D–0D MoS2–PbS quantum dot photodetectors. Advanced materials, 27(1), pp.176-180.

18. Yasaei, P., Kumar, B., Foroozan, T., Wang, C., Asadi, M., Tuschel, D., Indacochea, J.E., Klie, R.F. and Salehi-Khojin, A., 2015. High-quality black phosphorus atomic layers by liquid-phase exfoliation. Advanced Materials, 27(11), pp.1887-1892.

19. Zhou, J., Lin, J., Huang, X., Zhou, Y., Chen, Y., Xia, J., Wang, H., Xie, Y., Yu, H., Lei, J. and Wu, D., 2018. A library of atomically thin metal chalcogenides. Nature, 556(7701), p.355.

20. Chen, J., Tang, W., Tian, B., Liu, B., Zhao, X., Liu, Y., Ren, T., Liu, W., Geng, D., Jeong, H.Y. and Shin, H.S., 2016. Chemical vapor deposition of high-quality large-sized MoS2 crystals on silicon dioxide substrates. Advanced Science, 3(8), p.1500033.

21. Lee, Y.H., Zhang, X.Q., Zhang, W., Chang, M.T., Lin, C.T., Chang, K.D., Yu, Y.C., Wang, J.T.W., Chang, C.S., Li, L.J. and Lin, T.W., 2012. Synthesis of large-area MoS2 atomic layers with chemical vapor deposition. Advanced materials, 24(17), pp.2320-2325.

22. Yang, S.Y., Shim, G.W., Seo, S.B. and Choi, S.Y., 2017. Effective shape-controlled growth of monolayer MoS 2 flakes by powder-based chemical vapor deposition. Nano Research, 10(1), pp.255-262.

23. O'Brien, M., McEvoy, N., Motta, C., Zheng, J.Y., Berner, N.C., Kotakoski, J., Elibol, K., Pennycook, T.J., Meyer, J.C., Yim, C. and Abid, M., 2016. Raman characterization of platinum diselenide thin films. 2D Materials, 3(2), p.021004.

24. Zeng, L.H., Wu, D., Lin, S.H., Xie, C., Yuan, H.Y., Lu, W., Lau, S.P., Chai, Y., Luo, L.B., Li, Z.J. and Tsang, Y.H., 2019. Controlled Synthesis of 2D Palladium Diselenide for Sensitive Photodetector Applications. Advanced Functional Materials, 29(1), p.1806878.

25. Lin, S., Liu, Y., Hu, Z., Lu, W., Mak, C.H., Zeng, L., Zhao, J., Li, Y., Yan, F., Tsang, Y.H. and Zhang, X., 2017. Tunable active edge sites in PtSe2 films towards hydrogen evolution reaction. Nano Energy, 42, pp.26-33.

26. Oyedele, A.D., Yang, S., Liang, L., Puretzky, A.A., Wang, K., Zhang, J., Yu, P., Pudasaini, P.R., Ghosh, A.W., Liu, Z. and Rouleau, C.M., 2017. PdSe2: Pentagonal two-dimensional layers with high air stability for electronics. Journal of the American Chemical Society, 139(40), pp.14090-14097.

27. Roberts, A.C., Paar, W.H., Cooper, M.A., Topa, D., Criddle, A.J. and Jedwab, J., 2002. Verbeekite, monoclinic PdSe2, a new mineral from the Musonoi Cu-Co-Mn-U mine, near Kolwezi, Shaba Province, Democratic Republic of Congo. Mineralogical Magazine, 66(1), pp.173-179.

28. Long, M., Wang, Y., Wang, P., Zhou, X., Xia, H., Luo, C., Huang, S., Zhang, G., Yan, H., Fan, Z. and Wu, X., 2019. Palladium diselenide long-wavelength infrared photodetector with high sensitivity and stability. ACS nano, 13(2), pp.2511-2519.

29. Chow, W.L., Yu, P., Liu, F., Hong, J., Wang, X., Zeng, Q., Hsu, C.H., Zhu, C., Zhou, J., Wang, X. and Xia, J., 2017. High mobility 2D palladium diselenide field-effect transistors with tunable ambipolar characteristics. Advanced Materials, 29(21), p.1602969.

30. Zeng, L., Tao, L., Tang, C., Zhou, B., Long, H., Chai, Y., Lau, S.P. and Tsang, Y.H., 2016. High-responsivity UV-vis photodetector based on transferable WS 2 film deposited by magnetron sputtering. Scientific reports, 6, p.20343.

31. Zhang, G., Amani, M., Chaturvedi, A., Tan, C., Bullock, J., Song, X., Kim, H., Lien, D.H., Scott, M.C., Zhang, H. and Javey, A., 2019. Optical and electrical properties of two-dimensional palladium diselenide. Applied Physics Letters, 114(25), p.253102.

32. Late, D.J., Liu, B., Matte, H.R., Dravid, V.P. and Rao, C.N.R., 2012. Hysteresis in single-layer MoS2 field effect transistors. ACS nano, 6(6), pp.5635-5641.

33. Wang, A., Yan, X., Zhang, M., Sun, S., Yang, M., Shen, W., Pan, X., Wang, P. and Deng, Z., 2016. Controlled synthesis of lead-free and stable perovskite derivative Cs2SnI6 nanocrystals via a facile hot-injection process. Chemistry of Materials, 28(22), pp.8132-8140.

34. Bube, R. H., 1992. Photoelectronic Properties of Semiconductors, Cambridge University Press: Cambridge, U.K.,

35. Šnejdar, V., & Jerhot, J., 1976. Electrical conductivity of polycrystalline semiconductors. Thin Solid Films, 37(3), 303-316.

36. Sugahara, T., Sato, H., Hao, M., Naoi, Y., Kurai, S., Tottori, S., Kenji, Y., Katsushi, N., Linda. T. R. and Sakai, S.,1998. Direct evidence that dislocations are non-radiative recombination centers in GaN. Japanese journal of applied physics, 37(4A), L398.

37. Street, R. A., 1977. Non-radiative recombination in chalcogenide glasses. Solid State Communications, 24(5), 363-365.

38. Li, J., Niu, L., Zheng, Z., & Yan, F., 2014. Photosensitive graphene transistors. Advanced Materials, 26(31), 5239-5273.

39. Xie, C., You, P., Liu, Z., Li, L. and Yan, F., 2017. Ultrasensitive broadband phototransistors based on perovskite/organic-semiconductor vertical heterojunctions. Light: Science & Applications, 6(8), p.e17023.

40. Ni, Z., Ma, L., Du, S., Xu, Y., Yuan, M., Fang, H., Wang, Z., Xu, M., Li, D., Yang, J. and Hu, W., 2017. Plasmonic silicon quantum dots enabled high-sensitivity ultrabroadband photodetection of graphene-based hybrid phototransistors. ACS nano, 11(10), pp.9854-9862.

41. Zhou, X., Zhang, Q., Gan, L., Li, H. and Zhai, T., 2016. Large-Size Growth of Ultrathin SnS2 Nanosheets and High Performance for Phototransistors. Advanced Functional Materials, 26(24), pp.4405-4413.

42. Liang, Q., Wang, Q., Zhang, Q., Wei, J., Lim, S. X., Zhu, R., Hu, J., Wei, W., Lee, C., Sow, C., Zhang. W. & Wew, A.T.S., 2019. High-Performance, Room Temperature, Ultra-Broadband Photodetectors Based on Air-Stable PdSe2. Advanced Materials, 31(24), 1807609.

43. Jung, C., Kim, S.M., Moon, H., Han, G., Kwon, J., Hong, Y.K., Omkaram, I., Yoon, Y., Kim, S. and Park, J., 2015. Highly crystalline CVD-grown multilayer MoSe 2 thin film transistor for fast photodetector. Scientific reports, 5, p.15313.

44. Chen, J., Liu, B., Liu, Y., Tang, W., Nai, C.T., Li, L., Zheng, J., Gao, L., Zheng, Y., Shin, H.S. and Jeong, H.Y., 2015. Chemical Vapor Deposition of Large-Sized Hexagonal WSe2 Crystals on Dielectric Substrates. Advanced materials, 27(42), pp.6722-6727.

45. Perea-López, N., Lin, Z., Pradhan, N.R., Iñiguez-Rábago, A., Elías, A.L., McCreary, A., Lou, J., Ajayan, P.M., Terrones, H., Balicas, L. and Terrones, M., 2014. CVD-grown monolayered MoS2 as an effective photosensor operating at low-voltage. 2D Materials, 1(1), p.011004.

46. Zhang, W., Huang, J.K., Chen, C.H., Chang, Y.H., Cheng, Y.J. and Li, L.J., 2013. High-gain phototransistors based on a CVD MoS2 monolayer. Advanced materials, 25(25), pp.3456-3461.

47. Huang, Y., Xu, K., Wang, Z., Shifa, T.A., Wang, Q., Wang, F., Jiang, C. and He, J., 2015. Designing the shape evolution of SnSe 2 nanosheets and their optoelectronic properties. Nanoscale, 7(41), pp.17375-17380.

48. Zhang, E., Jin, Y., Yuan, X., Wang, W., Zhang, C., Tang, L., Liu, S., Zhou, P., Hu, W. and Xiu, F., 2015. ReS2-Based Field-Effect Transistors and Photodetectors. Advanced Functional Materials, 25(26), pp.4076-4082.

Supporting Information

Photoresponse of wafer-scale palladium diselenide films prepared by selenization method

Chun Hin Mak, Shenghuang Lin, Lukas Rogée and Shu Ping Lau

Department of Applied Physics, The Hong Kong Polytechnic University,
Hung Hom, Kowloon, Hong Kong SAR

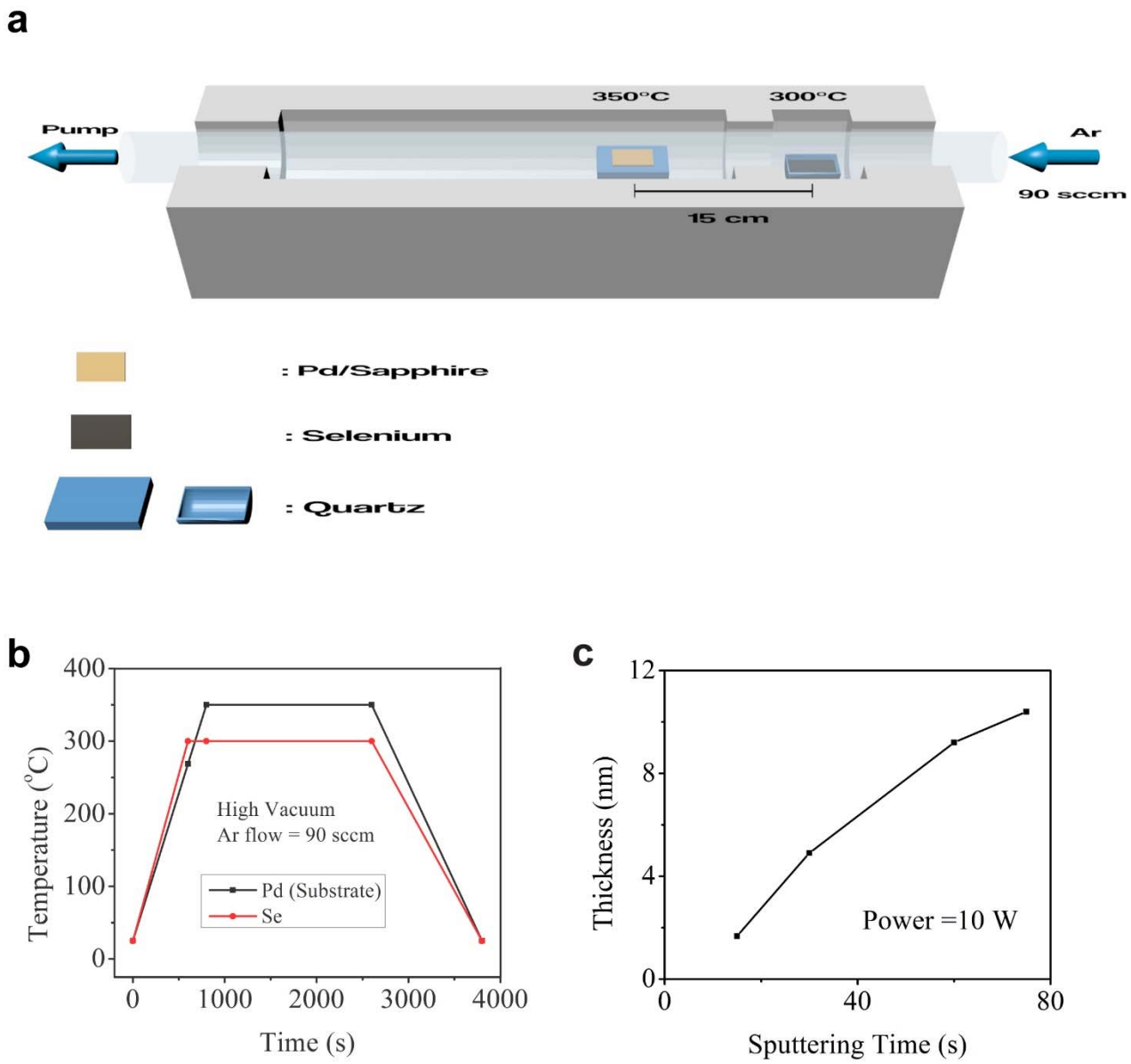

Figure S1 (a) Illustration of the selenization process. (b) Temperature profile of the selenization process. (c) The thickness of the $PdSe_2$ film as a function of Pd sputtering time.

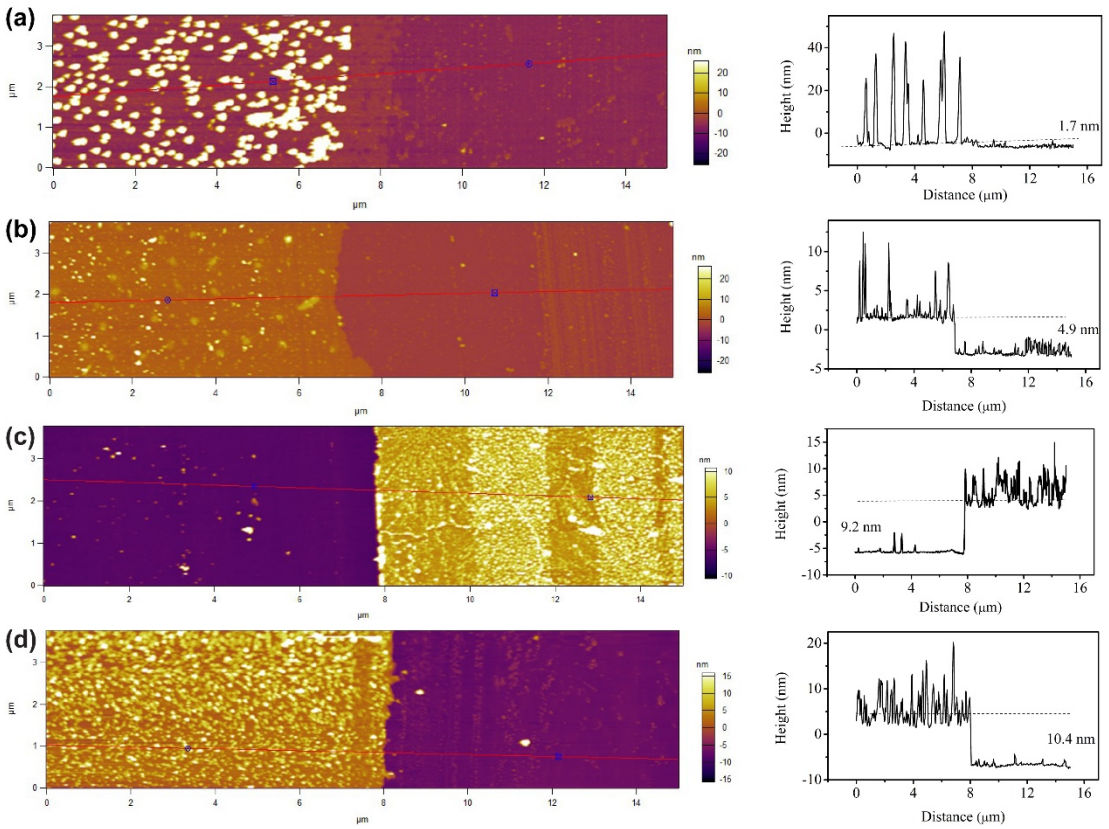

Figure S2 AFM measurement of the $PdSe_2$ films for different Pd deposition times: A) 15s, B) 30s, C) 60s and D) 75s.

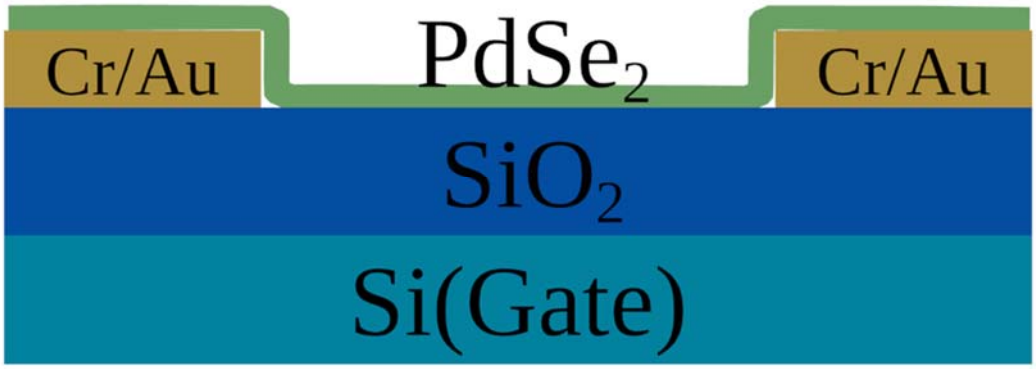

Figure S3 Schematic diagram of the $PdSe_2$ transistor.

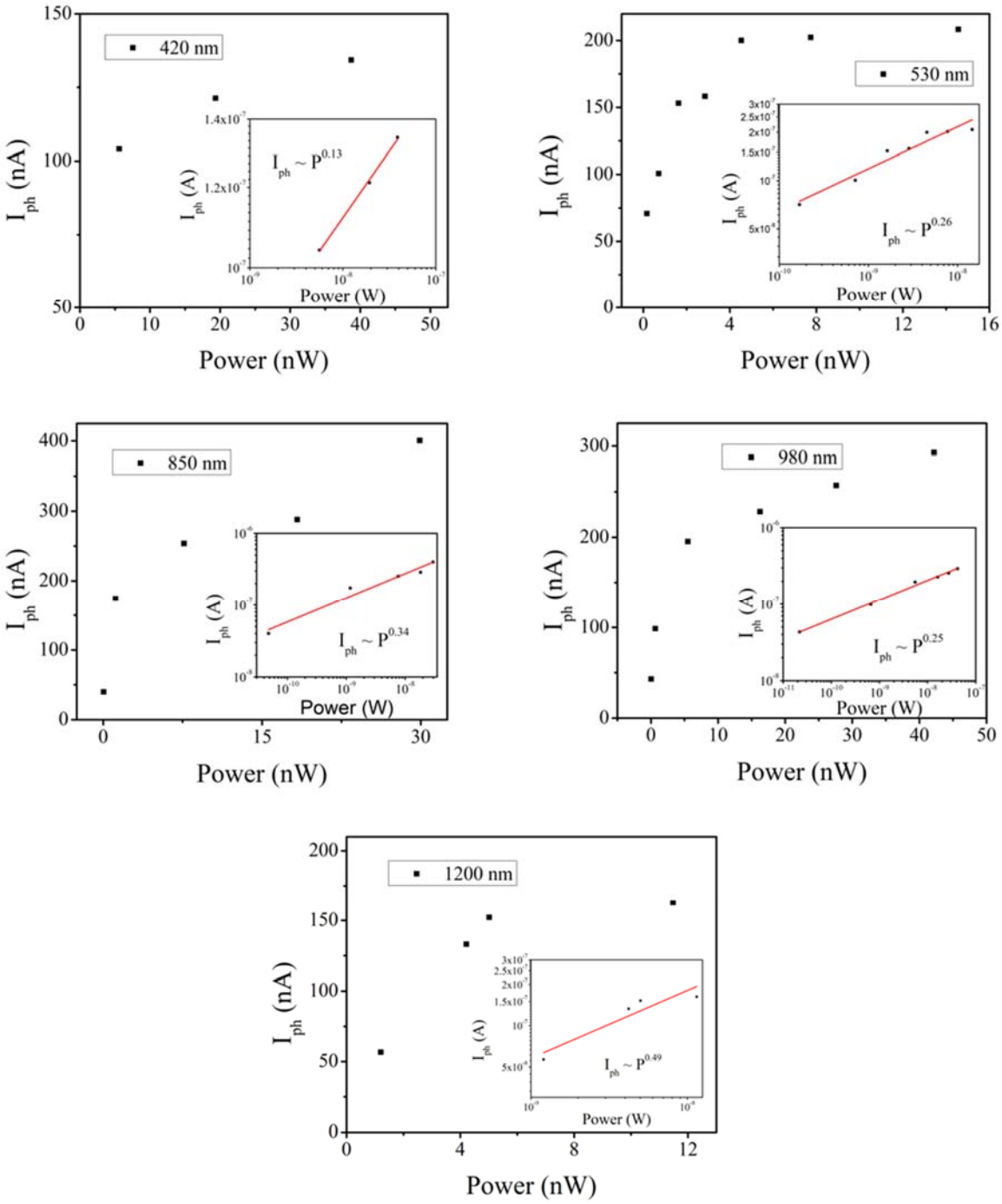

Figure S4 Photocurrent and power relationship in linear and logarithm scale. Linear relationship in logarithm scale are found in all sensing wavelength.

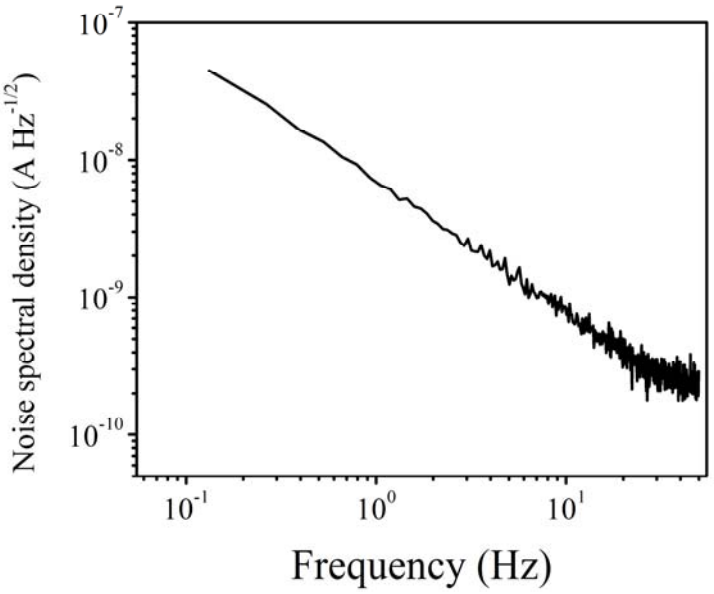

Figure S5 Analysis of noise spectral density of the device by the FFT of the dark current noise. The noise currents were measured at V_{DS} = 3V.

After the FFT analysis of the noise current, the 1/f noise spectral densities of the FET at the bandwidth B = 1 Hz is ~722 pAHz$^{-1/2}$.